Analysis of laterally loaded monopiles: a non-linear elastic approach

B.K. Gupta & D. Basu
University of Waterloo, Ontario, Canada

ABSTRACT: The objective of this paper is to describe a new continuum-based analysis for predicting the nonlinear response of laterally loaded monopiles. In the analysis, the monopile is modelled as an elastic Euler-Bernoulli beam and the soil as a continuum, which is characterized by nonlinear elastic relationships. The soil displacements are assumed to be a product of separable functions and the principle of virtual work is applied to obtain the governing differential equations describing the pile and soil displacements, which are solved using the one-dimensional finite difference method in an iterative scheme. The reliability of the results obtained from the present analysis is validated against the results obtained from field pile-load tests and the results obtained from the *p-y* analysis of piles embedded in clayey and sandy soil deposits.

1 INTRODUCTION

For the analysis and design of laterally loaded pile foundations, the two commonly used methods are (i) nonlinear Winkler spring-based *p-y* method (Reese et al. 1975, O'Neill et al. 1990) and (ii) three dimensional (3-D) continuum-based method with finite element (FE) solutions (Trochanis et al. 1991, Achmus et al. 2009) obtained using commercially available software packages. The *p-y* method is popular because it is mathematically simple and computationally inexpensive. However, the *p-y* curves consider only the compressive resistance of soil and neglects the soil shear resistance, thus oversimplifying the continuum nature of the pile-soil interaction problem. Besides, the *p-y* curves are site-specific and dependant on empirical constants that are arbitrarily determined by users based on experience. The continuum-based methods, on the other hand, are appealing to researchers because these methods can handle various geometries, boundary conditions, and can incorporate sophisticated elasto-plastic soil constitutive models. However, the continuum-based 3-D FE analysis are often computationally expensive and require specific skills to run the software packages.

For laterally loaded monopiles and piles, 3-D elasto-plastic analysis may not be necessary because the primary design interest for most laterally loaded pile problems is the estimation of head displacement and/or rotation under working load conditions (e.g., maximum tolerable head displacement of 25 mm for slender piles or maximum head rotation of 0.25° for large-diameter monopiles is often the design criterion). In order to capture the pile behaviour based on these design criteria, nonlinear elastic analysis instead of elasto-plastic analysis is sufficient.

The objective of this paper is to present the formulation of an alternate continuum-based method for the analysis of laterally loaded monopile foundations. In the analysis, the monopile is assumed to behave as an elastic Euler-Bernoulli beam and the soil is characterized by a nonlinear elastic constitutive relationship. The displacement within the soil mass is considered to be a product of separable functions and the principle of virtual work is applied to obtain the governing differential equations describing the monopile and soil displacements, which are solved using a one-dimensional (1-D) finite difference (FD) method following an iterative scheme. The accuracy of this formulation is ensured by comparing the pile responses obtained from the present analysis with those from field pile-load tests and from *p-y* analysis.

2 CONSTITUTIVE MODEL FOR CLAY AND SAND

Vardanega and Bolton (2013) proposed a nonlinear elastic modulus reduction relationship for clayey soils for use in the foundation engineering practice, which is given by

$$G_s = \frac{G_{s0}}{1+\left(\frac{\gamma_{\text{oct}}}{\gamma_{\text{ref}}}\right)^{\alpha}} \tag{1}$$

where G_s is the secant shear modulus at any strain, G_{s0} is the initial (small-strain or elastic) shear modulus, α (= 0.736) is the curvature parameter describing the nonlinear variation of shear modulus with soil strain, γ_{ref} (= $J \times$ PI/1000; in which J = 2.2 and PI = plasticity index of clay expressed as a fraction) is the octahedral reference shear strain of soil at which the G_{s0} is halved and γ_{oct} is the octahedral engineering shear strain in soil at a point where G_s is determined, and is given by

$$\gamma_{oct} = \frac{2}{3}\left[\left(\varepsilon_{rr}-\varepsilon_{\theta\theta}\right)^2+\left(\varepsilon_{\theta\theta}-\varepsilon_{zz}\right)^2+\left(\varepsilon_{zz}-\varepsilon_{rr}\right)^2 +6\left(\varepsilon_{r\theta}^2+\varepsilon_{\theta z}^2+\varepsilon_{zr}^2\right)\right]^{\frac{1}{2}} \quad (2)$$

in which ε_{rr}, $\varepsilon_{\theta\theta}$, ε_{zz}, $\varepsilon_{r\theta}$, $\varepsilon_{\theta z}$, and ε_{zr} are the components of 3-D strain state in soil described with respect to a cylindrical r-θ-z coordinate system. Considering a total stress approach for undrained clay, G_{s0} is obtained in this paper from the undrained shear strength of clay s_u following a correlation that Duncan and Buchignani (1976) proposed (also included in USACE 1990):

$$G_{s0} = 0.33 K_c s_u \quad (3)$$

where s_u is the undrained shear strength, and the dimensionless coefficient K_c depends on PI (expressed as percent) and overconsolidation ratio OCR, and can be obtained from Figure 1. It is assumed that clay Poisson's ratio $\nu_s \approx 0.5$, representing zero volume change under undrained condition, while relating G_{s0} to s_u in Equation 3.

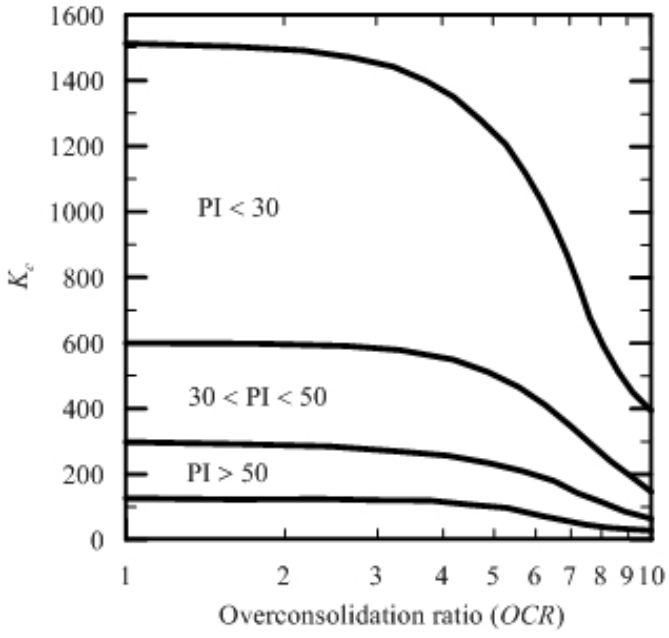

Figure 1. Relationship between K_c, PI, and OCR for undrained clays (Regenerated from USACE (1990))

Oztoprak and Bolton (2013) formulated a similar nonlinear elastic modulus reduction equation from the shear stress-strain data of sandy soils, which is given by

$$G_s = \frac{G_{s0}}{1+\left(\frac{\gamma_{oct}-\gamma_e}{\gamma_{ref}}\right)^{\alpha}} \quad (4)$$

where γ_e is the elastic threshold strain beyond which the shear modulus falls below its maximum, γ_{ref} is the characteristic reference strain at which the initial shear modulus is halved, and for $\gamma_{oct} < \gamma_e$, $G_s/G_{s0} = 1$. The numerical values of γ_e, γ_{ref}, and α are reported in Table 1.

In this paper, G_{s0} for a sandy soil deposit is evaluated from the following equation given by Hardin and Black (1966)

$$\frac{G_{s0}}{p_a} = C_g \frac{\left(e_g - e_0\right)^2}{1+e_0}\left(\frac{\sigma'_{m0}}{p_a}\right)^{n_g} \quad (5)$$

where C_g, e_g, and n_g are intrinsic soil properties (C_g = 612.0, e_g = 2.17, and n_g = 0.44 corresponding to Ottawa sand); σ'_{m0} is the initial mean effective stress, p_a is the reference stress (= 100 kPa), and e_0 is the initial void ratio.

Table 1. Fitted parameters for lower bound, mean, and upper bound curves corresponding to Equation (4) (see plot in Figure 2)

Parameters	Lower bound	Mean	Upper bound
γ_{ref}	0.0002	0.00044	0.001
γ_e	0	0.000007	0.00003
α	0.88	0.88	0.88

3 PROBLEM DEFINITION

Figure 1 shows a circular monopile of length L_p, radius r_p, area of cross-section A_p, second moment of inertia I_p, and characterized by Young's modulus E_p embedded in a soil deposit. The monopile is assumed to behave as an elastic Euler-Bernoulli beam and the soil deposit is isotropic and characterized by the nonlinear modulus reduction relationship given by Equation 1 or 4. The soil layer extends to an infinite distance along the radial and vertical directions. A cylindrical r-θ-z coordinate system is chosen for the purpose of analysis in which the origin of the coordinate system lies at the center of the pile head and the z-axis points downward and coincide with the pile axis. No slippage or separation between the pile and the surrounding soil is assumed. The objective of the analysis is to predict the nonlinear pile response – displacement w and rotation dw/dz under the action of static horizontal force F_a and/or moment M_a at the pile head.

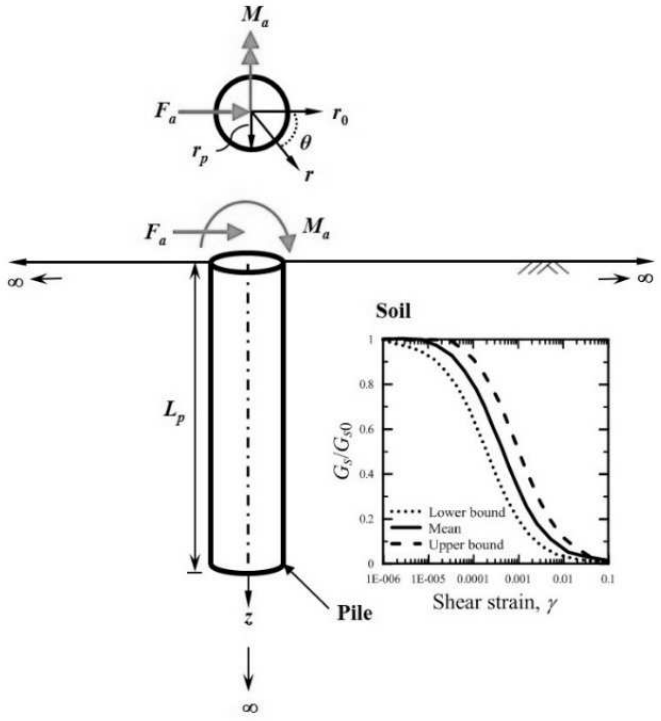

Figure 2. Laterally loaded monopile embedded in a spatially varying soil deposit

4 MATHEMATICAL FORMULATION

The vertical soil displacement u_z is neglected and the horizontal soil displacements u_r and u_θ in the radial and tangential directions are expressed as products of separable functions as (Basu et al. 2009, Gupta 2018)

$$u_r(r,\theta,z) = w(z)\phi_r(r)\cos\theta \tag{6}$$

$$u_\theta(r,\theta,z) = -w(z)\phi_\theta(r)\sin\theta \tag{7}$$

where ϕ_r and ϕ_θ are dimensionless functions of the radial coordinate that are both assumed to be equal to 1.0 at $r = r_p$ and equal to zero at $r = \infty$.

Applying the principle of virtual work to the pile-soil system, which is subjected to a static force F_a and/or moment M_a at the pile head (Fig. 2), the following equation is obtained

$$E_pI_p\int_0^{L_p}\left(\frac{d^2w}{dz^2}\right)\delta\left(\frac{d^2w}{dz^2}\right)dz+\int_0^{\infty}\int_0^{2\pi}\int_{r_p}^{\infty}\sigma_{pq}\delta\varepsilon_{pq}\,r\,dr\,d\theta\,dz$$
$$+\int_{L_p}^{\infty}\int_0^{2\pi}\int_0^{r_p}\sigma_{pq}\delta\varepsilon_{pq}\,r\,dr\,d\theta\,dz-F_a\,\delta w\big|_{z=0}+M_a\delta\left(\frac{dw}{dz}\right)\Big|_{z=0}=0 \tag{8}$$

where the first, second, and third integrals on the left-hand side of Equation (8) denote the internal virtual works done by the pile, the soil excluding the cylindrical soil domain below the pile base, and the cylindrical soil of radius r_p below the pile base, respectively. The fourth and the fifth terms on the left-hand side of Equation 8 denote the external work done by the applied force and moment, respectively.

Further, considering the assumed soil displacement field (Eqs 6 and 7) the infinitesimal components of the strain tensor ε_{pq} and stress tensor σ_{pq} [$= \lambda_s\delta_{pq}\varepsilon_{ll} + 2G_s\varepsilon_{pq}$ (λ_s and G_s are the Lame's constants and δ_{pq} is the Kronecker's delta)] at any point within the soil mass are obtained, which are substituted in Equation 8 to obtain the following:

$$E_pI_p\int_0^{L_p}\left(\frac{d^2w}{dz^2}\right)\delta\left(\frac{d^2w}{dz^2}\right)dz+\int_{L_p}^{\infty}\pi r_p^2G_{s0}\left(\frac{dw}{dz}\right)\delta\left(\frac{dw}{dz}\right)dz$$
$$+\int_0^{\infty}\int_0^{2\pi}\int_{r_p}^{\infty}\Bigg\{(\lambda_s+2G_s)\left(\frac{d\phi_r}{dr}\right)^2\cos^2\theta+G_s\left(\frac{\phi_r-\phi_\theta}{r}\right)^2\sin^2\theta$$
$$+2\lambda_s\frac{d\phi_r}{dr}\left(\frac{\phi_r-\phi_\theta}{r}\right)\cos^2\theta+(\lambda_s+2G_s)\left(\frac{\phi_r-\phi_\theta}{r}\right)^2\cos^2\theta$$
$$+2G_s\frac{d\phi_\theta}{dr}\left(\frac{\phi_r-\phi_\theta}{r}\right)\sin^2\theta+G_s\left(\frac{d\phi_r}{dr}\right)^2\sin^2\theta\Bigg\}w\delta w\,r\,dr\,d\theta\,dz$$
$$+\int_0^{\infty}\int_0^{2\pi}\int_{r_p}^{\infty}\left\{G_s\phi_\theta^2\sin^2\theta+G_s\phi_r^2\cos^2\theta\right\}\left(\frac{dw}{dz}\right)\delta\left(\frac{dw}{dz}\right)r\,dr\,d\theta\,dz$$
$$-F_a\,\delta w\big|_{z=0}+M_a\delta\left(\frac{dw}{dz}\right)\Big|_{z=0}+\int_0^{\infty}\int_0^{2\pi}\int_{r_p}^{\infty}\Bigg\{\lambda_sw^2\cos^2\theta\left(\frac{\phi_r-\phi_\theta}{r}\right)$$
$$+(\lambda_s+2G_s)w^2\cos^2\theta\frac{d\phi_r}{dr}\Bigg\}\delta\left(\frac{d\phi_r}{dz}\right)r\,dr\,d\theta\,dz$$
$$+\int_0^{\infty}\int_0^{2\pi}\int_{r_p}^{\infty}\Bigg\{(\lambda_s+2G_s)\frac{w^2}{r^2}(\phi_r-\phi_\theta)\cos^2\theta$$
$$+\lambda_s\frac{w^2}{r}\frac{d\phi_r}{dr}\cos^2\theta+G_s\frac{w^2}{r^2}(\phi_r-\phi_\theta)\sin^2\theta$$
$$+G_s\frac{w^2}{r}\sin^2\theta\frac{d\phi_\theta}{dr}+G_s\left(\frac{dw}{dz}\right)^2\cos^2\theta\,\phi_r\Bigg\}\delta\phi_r\,r\,dr\,d\theta\,dz$$
$$+\int_0^{\infty}\int_0^{2\pi}\int_{r_p}^{\infty}\Bigg\{G_sw^2\sin^2\theta\left(\frac{\phi_r-\phi_\theta}{r}\right)$$
$$+G_sw^2\sin^2\theta\frac{d\phi_\theta}{dr}\Bigg\}\delta\left(\frac{d\phi_\theta}{dz}\right)r\,dr\,d\theta\,dz$$
$$+\int_0^{\infty}\int_0^{2\pi}\int_{r_p}^{\infty}\Bigg\{-(\lambda_s+2G_s)\frac{w^2}{r^2}(\phi_r-\phi_\theta)\cos^2\theta$$
$$-\lambda_s\frac{w^2}{r}\frac{d\phi_r}{dr}\cos^2\theta-G_s\frac{w^2}{r^2}(\phi_r-\phi_\theta)\sin^2\theta$$
$$-G_s\frac{w^2}{r}\sin^2\theta\frac{d\phi_\theta}{dr}+G_s\left(\frac{dw}{dz}\right)^2\sin^2\theta\,\phi_\theta\Bigg\}\delta\phi_\theta\,r\,dr\,d\theta\,dz=0 \tag{9}$$

It is assumed in Equation 9 that the soil deposit is heterogeneous with spatially varying elastic constants λ_s [$= 2G_s(1-\nu_s)/(1-2\nu_s)$] and G_s [$= E_s/\{2(1+\nu_s)\}$] (E_s = soil Young's modulus and ν_s = soil Poisson's ratio). This implies that these parameters are functions of the radial coordinate r and tangential coordinate θ (i.e., $\lambda_s = \lambda_s(r,\theta)$ and $G_s = G_s(r,\theta)$) and therefore, included within the integrations. The assumption of spatially varying λ_s and G_s is required for the development of the nonlinear analysis framework because the reduction of soil modulus as a function of strain renders the soil heterogeneous under applied loading even if the

soil deposit is homogeneous in situ. Further, for the circular soil domain of radius r_p below the pile base, the spatial variation of λ_s and G_s is neglected because the soil stiffness is not expected to degrade much within this region.

Considering the variation of w, ϕ_r, and ϕ_θ in Equation 9, the following differential equations are obtained

$$2t_n \frac{d^2 w_n}{dz^2} - k w_n = 0 \tag{10}$$

$$E_p I_p \frac{d^4 w}{dz^4} - 2t \frac{d^2 w}{dz^2} + kw = 0 \tag{11}$$

$$\frac{d^2 \phi_r}{dr^2} + \gamma_1 \frac{d\phi_r}{dr} - \gamma_2 \phi_r = \gamma_3 \frac{d\phi_\theta}{dr} - \gamma_4 \phi_\theta \tag{12}$$

$$\frac{d^2 \phi_\theta}{dr^2} + \gamma_5 \frac{d\phi_\theta}{dr} - \gamma_6 \phi_\theta = -\gamma_7 \frac{d\phi_r}{dr} - \gamma_8 \phi_r \tag{13}$$

along with the relevant boundary conditions (for details see Gupta 2018). Equations 10 and 11 are the governing differential equations of the cylindrical soil domain of radius r_p below the pile base ($L_p \le z \le \infty$) and the pile ($0 \le z \le L_p$), respectively, while Equations 12 and 13 are the governing differential equations for the soil displacement functions. Further, in Equations 10-13:

$$\begin{aligned} k = \int_0^{2\pi}\int_{r_p}^{\infty} \Bigg\{ & (\lambda_s + 2G_s)\left(\frac{d\phi_r}{dr}\right)^2 \cos^2\theta + G_s r \left(\frac{d\phi_\theta}{dr}\right)^2 \sin^2\theta \\ & + 2\lambda_s \left(\frac{\phi_r - \phi_\theta}{r}\right)\frac{d\phi_r}{dr}\cos^2\theta + (\lambda_s + 2G_s)\left(\frac{\phi_r - \phi_\theta}{r}\right)^2 \cos^2\theta \\ & + G_s \left(\frac{\phi_r - \phi_\theta}{r}\right)^2 \sin^2\theta + G_s \left(\frac{\phi_r - \phi_\theta}{r}\right)\frac{d\phi_\theta}{dr}\sin^2\theta \Bigg\} r dr d\theta \end{aligned} \tag{14}$$

$$t = \frac{1}{2}\int_0^{2\pi}\int_{r_p}^{\infty} G_s \left(\phi_r^2 \cos^2\theta + \phi_\theta^2 \sin^2\theta\right) r dr d\theta \tag{15}$$

$$t_n = \frac{1}{2}\int_0^{2\pi}\int_{r_p}^{\infty} G_s \left(\phi_r^2 \cos^2\theta + \phi_\theta^2 \sin^2\theta\right) r dr d\theta + \frac{\pi}{2} r_p^2 G_{s0} \tag{16}$$

$$\gamma_1 = \frac{1}{m_{s1}}\frac{dm_{s1}}{dr} \tag{17}$$

$$\gamma_2 = \frac{1}{r^2}\left(\frac{m_{s1} + m_{s2} + m_{s3}}{m_{s1}}\right) - \frac{1}{r\, m_{s1}}\frac{dm_{s3}}{dr} + \left(\frac{n_{s1}}{m_{s1}}\right) \tag{18}$$

$$\gamma_3 = \frac{1}{r}\left(\frac{m_{s2} + m_{s3}}{m_{s1}}\right) \tag{19}$$

$$\gamma_4 = \frac{1}{r^2}\left(\frac{m_{s1} + m_{s2} + m_{s3}}{m_{s1}}\right) - \frac{1}{r\, m_{s1}}\frac{dm_{s3}}{dr} \tag{20}$$

$$\gamma_5 = \frac{1}{m_{s2}}\frac{dm_{s2}}{dr} \tag{21}$$

$$\gamma_6 = \frac{1}{r^2}\left(\frac{m_{s1}}{m_{s2}}\right) + \frac{1}{r\, m_{s2}}\frac{dm_{s2}}{dr} + \left(\frac{n_{s2}}{m_{s2}}\right) \tag{22}$$

$$\gamma_7 = \frac{1}{r}\left(\frac{m_{s2} + m_{s3}}{m_{s2}}\right) \tag{23}$$

$$\gamma_8 = \frac{1}{r^2}\frac{m_{s1}}{m_{s2}} + \frac{1}{r\, m_{s2}}\frac{dm_{s2}}{dr} \tag{24}$$

where m_{s1}, m_{s2}, m_{s3}, n_{s1}, and n_{s2} in Equations 17-24 are given by:

$$m_{s1} = \int_0^{\infty}\int_0^{2\pi} (\lambda_s + 2G_s) w^2 \cos^2\theta\, r d\theta dz \tag{25}$$

$$m_{s2} = \int_0^{\infty}\int_0^{2\pi} G_s w^2 \sin^2\theta\, r d\theta dz \tag{26}$$

$$m_{s3} = \int_0^{\infty}\int_0^{2\pi} \lambda_s w^2 \cos^2\theta\, r d\theta dz \tag{27}$$

$$n_{s1} = \int_0^{\infty}\int_0^{2\pi} G_s \left(\frac{dw}{dz}\right)^2 \cos^2\theta\, r d\theta dz \tag{28}$$

$$n_{s2} = \int_0^{\infty}\int_0^{2\pi} G_s \left(\frac{dw}{dz}\right)^2 \sin^2\theta\, r d\theta dz \tag{29}$$

5 SOLUTION ALGORITHM

The soil parameters k and t, which are functions of ϕ_r and ϕ_θ, must be known to obtain w from Equations 10-11 describing the pile displacement. Moreover, the parameters γ_1-γ_8 must be known to obtain ϕ_r and ϕ_θ, and these parameters depend on w through m_{s1}, m_{s2}, m_{s3}, n_{s1}, and n_{s2}. Therefore, the differential equations describing the pile displacement w and soil displacement functions ϕ_r and ϕ_θ are coupled, and an iterative algorithm is required to obtain solution. In order to obtain the w, the pile and the soil domain are discretized into 1-D FD nodes.

In the iterative algorithm an initial guess of 1.0 is made for γ_1-γ_8 at each node along the soil domain and the finite difference form of the coupled differential equation for ϕ_r and ϕ_θ are written, which are solved iteratively. After obtaining ϕ_r and ϕ_θ at each node, the strain components are calculated with which the secant shear modulus $G_s(r,\theta)$ are evaluated using Equation 1 or 4 at each node in the soil domain along r and θ and at each node along the pile length. Using the calculated values of $G_s(r,\theta)$, ϕ_r and ϕ_θ, the values of k and t are calculated at each node along the pile length using the trapezoidal rule of integration where

the integration is first performed along the r-direction followed by a subsequent integration over θ. With the calculated values of k and t at each node along the pile length, w and dw/dz are evaluated at each node along pile length (for details of the FD equation and solution procedure, see Gupta 2018). With the calculated values of w and dw/dz, the parameters m_{s1}, m_{s2}, m_{s3}, n_{s1}, and n_{s2} are evaluated numerically following the trapezoidal rule of integration along the θ and z-directions. First, the integration is performed along θ at any radial distance; the integrand obtained is further integrated along the z-direction. After obtaining m_{s1}, m_{s2}, m_{s3}, n_{s1}, and n_{s2}, new values of γ_1-γ_8 are evaluated at each node and compared with the corresponding assumed initial values. If the differences in the assumed and obtained values of γ_1-γ_8 are more than the prescribed tolerable limit of 0.001 at each node, the calculations described so far are repeated with the calculated values of γ_1-γ_8 as the new initial guess values. Iterations are continued until the values of γ_1-γ_8 between successive iterations fall below the prescribed limit at each node.

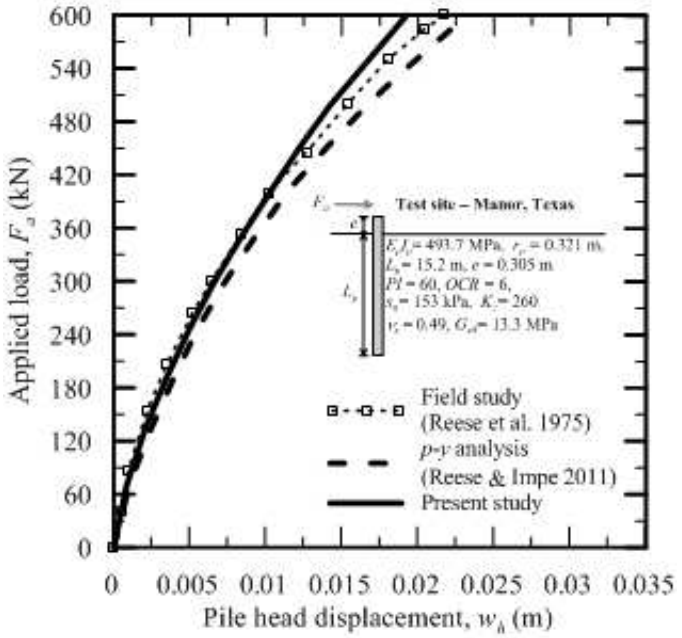

Figure 3. Comparison of pile head displacements obtained from full-scale field pile-load test at Manor, Texas test site, corresponding p-y analysis, and the present analysis simulating the test

6 RESULTS

The reliability and applicability of the present method using the nonlinear elastic soil models given by Equations 1 and 4 to predict laterally loaded pile response is demonstrated by comparing the predicted pile-head displacement obtained from the present analysis with those from field tests and p-y analysis.

Figure 3 shows the pile head displacement w_h obtained from a field test performed at a site in Manor, Texas, U.S.A. (Reese et al. 1975) and from the present analysis simulating the field test. The field test was performed on a small-diameter slender steel pipe pile with E_pI_p = 493.7 MPa, L_p = 15.2 m, r_p = 0.321 m, embedded in a heavily overconsolidated stiff undrained clayey soil deposit with s_u = 153 kPa, and PI = 60% (Guo 2013). The lateral load is applied at a height e = 0.305 m from the pile head. In order to simulate the pile response, an OCR of 6 is assumed (following Wu et al. 1998) for the clay deposit with K_c = 260 (from Fig. 2). This produces $G_{s0} = 0.34 \times K_c \times s_u = 0.33 \times 260 \times 153/1000 = 13.3$ MPa. Further, $\gamma_{s,\text{ref}} = J \times (\text{PI}/1000) = 2.2 \times (0.6/1000) = 0.00132$ is calculated for use in Equation 1. Also plotted in Figure 3 is the pile head response obtained from API-based (2011) p-y analysis (Reese & Impe 2011). From the comparison it is evident that the present analysis using Equation 1 is capable of predicting the field pile response in clayey soils quite well. Better prediction would be possible if more detailed site characterization is performed so that the parameters for the soil constitutive model can be determined with more certainty.

Figure 4 shows the comparison of pile head displacement w_h obtained from field pile-load test conducted at Arkansas river test site (Alizadeh & Davission 1970) on an small-diameter slender open-ended pipe pile (Pile 16), from the present analysis simulating the test, and from the corresponding p-y analysis following the API (2011) design code of practice (performed using the software package LPILE). For the comparison – an effective internal friction angle $\phi' = 43°$, effective unit of soil $\gamma' = 9.87$ kN/m^3 (Guo (2013)), and $\nu_s = 0.15$ are used as inputs for the sandy soil deposit; the pile properties and applied loading (reported by Guo 2013) are given in the figure itself (Fig. 4). To predict the response from the present formulation (i) $\sigma'_{m0} = (\sigma'_{zz} + 2 \times \sigma'_{rr})/3 = \sigma'_{zz} \times (1 + 2 \times K_0)/3 = \gamma' \times z \times (1 + 2 \times K_0)/3$ (where $\sigma'_{zz} = \gamma' \times z$ and $\sigma'_{rr} = K_0 \times \sigma'_{zz}$ are the effective vertical and horizontal stresses, respectively, at any depth z with K_0 (= 1 - sinϕ') = 0.32 is the coefficient of earth pressure at rest for a normally consolidated soil) is evaluated at each node along the pile length and (ii) G_{s0} is evaluated following Equation 3 for $e_0 = \{(\gamma_s/\gamma_w - 1) \times \gamma_w\}/\gamma' - 1 = \{(2.65 - 1) \times 9.81\}/9.87 - 1 = 0.64$ (γ_w = 9.81 kN/m^3 is the unit weight of water and γ_s = 2.65 kN/m^3 is the unit weight of sand solids), C_g = 612.0, e_g = 2.17, and n_g = 0.44 corresponding to Ottawa sand, and (iii) Equation 4 with γ_{ref}, γ_e, and α corresponding to the upper bound curve (see Table 1 and the plot in Fig. 2) are used as the friction angle of the sandy soil deposit corresponds to that of dense sand (Budhu 2010) and it is expected that the rate of reduction of soil modulus for dense sand would be slower than that of medium (mean curve) and loose (lower bound curve) sand. The results for the p-y analysis is obtained for an initial modulus of subgrade

reaction k_h = 46.15 MN/m^3 corresponding to ϕ' = 43° and sand below the water table in the LPILE software. From the comparison it can be inferred that, using the present analysis, the pile response can be predicted reasonably well using Equation (4). The minor deviation in pile response obtained using the present analysis with that of the field response may be a result of (i) choice of the hyperbolic relationship (Eq. 4) used, which might not be completely applicable to the specific field tests and/or (ii) the uncertainty associated in the estimation of G_{s0} (Eq. 5) where the parameters (C_g, e_g, and n_g) corresponding to clean Ottawa sand are used; a better prediction may be expected if appropriate numerical values of the parameters C_g, e_g, and n_g for sandy soils with fines are used for comparison.

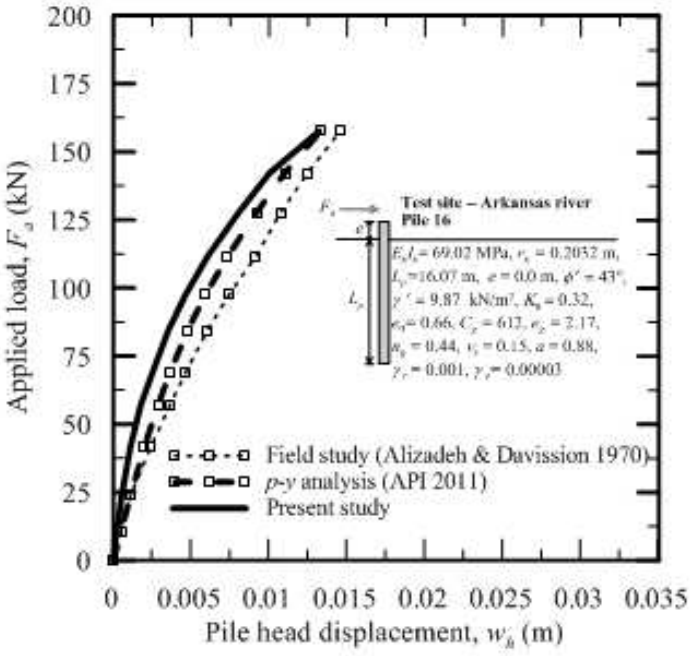

Figure 4. Comparison of pile head displacements obtained from full-scale field pile-load test at the Arkansas river (Pile 16) test site, corresponding *p-y* analysis (API 2011), and the present analysis simulating the field test

7 CONCLUSIONS

A new continuum-based formulation for the analysis of laterally loaded monopile foundations is developed. The monopile is assumed to be an elastic Euler-Bernoulli beam and the soil is modeled using nonlinear elastic constitutive relationships, which describe the reduction of secant shear modulus with induced shear strain within the soil. The displacements in the soil in the radial and tangential direction are expressed as products of separable functions and the principle of virtual work is applied to obtain the governing differential equations describing the monopile and soil displacements. 1-D finite difference solution of the differential equations describing the monopile and soil displacements are developed in conjunction with an iterative solution algorithm to obtain the monopile and soil displacements.

In order to demonstrate the reliability and applicability of the present analysis in predicting pile response in practice, the results obtained from the present analysis are compared with the results of full-scale field pile-load tests and corresponding *p-y* analysis. It is found that the present analysis can produce reasonably accurate results in practice.

8 REFERENCES

Achmus, M. Kuo, Y.S. & Abdel-Rahman, K. 2009. Behavior of monopile foundations under cyclic lateral load. *Computers and Geotechnics*. 36(5): 725-735.

Alizadeh, M. & Davisson, M.T. 1970. Lateral Load Tests on Piles—Arkansas River Project. *Journal of the Soil Mechanics and Foundations Division*, *ASCE*. 96(5): 1583-1604.

American Petroleum Institute (API). 2011. *Recommended practice for planning, designing and constructing fixed offshore platforms—Working stress design*. API Recommended Practice (RP 2A-WSD), 21st ed., Washington DC.

Basu, D. Salgado, R. & Prezzi, M. 2009. A continuum-based model for analysis of laterally loaded piles in layered soils. *Géotechnique*. 59(2): 127-140.

Budhu, M. 2010. *Soil mechanics and foundations*. 3rd edition, John Wiley & Sons, Inc., New York.

Duncan, J.M. & Buchignani, A.L. 1976. *An engineering manual for settlement studies*. University of California, Department of Civil Engineering.

Guo, W.D. 2013. Simple model for nonlinear response of 52 laterally loaded piles. *Journal of Geotechnical and Geoenvironmental Engineering*, *ASCE*. 139(2): 234-252.

Gupta, B.K. 2018. *Soil-Structure Interaction Analysis of Monopile Foundations Supporting Offshore Wind Turbines*. Doctoral dissertation, University of Waterloo.

Hardin, B.O. & Black, W.L. 1966. Sand Stiffness Under Various Triaxial Stresses. *Journal of the Soil Mechanics and Foundations Division*. 92(2): 27-42.

Oztoprak, S. & Bolton, M.D. 2013. Stiffness of sands through a laboratory test database. *Géotechnique*. 63(1): 54-70.

Reese, L.C. Cox, W.R. & Koop, F.D. 1975. Field testing and analysis of laterally loaded piles in stiff clay. In *Proc. 7th Offshore Technology Conference, Houston, Texas:* 672-690.

Reese, Lymon C. & William F. Van Impe. 2011. *Single Piles and Pile Groups Under Lateral Loading*. 2nd Edition, CRC Press, Taylor and Francis Group, London: UK.

Wu, D. Broms, B.B. & Choa, V. 1998. Design of laterally loaded piles in cohesive soils using py curves. *Soils and foundations*. *38*(2): 17-26.

Trochanis, A.M. Bielak, J. & Christiano, P. 1991. Three-dimensional nonlinear study of piles. *Journal of Geotechnical Engineering*. 117(3): 429-447.

USACE 1990. *Engineering and design: settlement analysis*. Engineer manual 1110–1–1904, US Army Corps of Engineers.

Vardanega, P.J. & Bolton, M.D. 2013. Stiffness of clays and silts: Normalizing shear modulus and shear strain. *Journal of Geotechnical and Geoenvironmental Engineering*. 139(9): 1575-1589.